

Supplementary Materials for

Highly efficient and stable platinum film deposited via a mixed metal-imidazole casting method as a benchmark cathode for electrocatalytic hydrogen evolution

Zaki N. Zahran,^{†‡*} Eman A. Mohamed,[†] Tomohiro Katsuki,[†] Yuta Tsubonouchi,[†] Debraj Chandra[†], Norihisa Hoshino[†] and Masayuki Yagi,^{†*}

[†]Department of Materials Science and Technology, Faculty of Engineering, Niigata University, 8050 Ikarashi-2, Niigata 9050-2181, Japan.

[‡]Faculty of Science, Tanta University, Tanta 511111, Egypt.

*Correspondence to: yagi@eng.niigata-u.ac.jp and znzahran@eng.niigata-u.ac.jp

Contents:

Table S1. Comparison of the Pt(*w*-MeIm) film with the state-of-the-art Pt-based catalysts for HER performance.

Figure S1. Photos of H₂PtCl₆ precursor solutions in MeOH and MeOH/MeIm.

Figure S2. Comparison of LSVs of the Pt(*w*-MeIm) film on GC electrodes as measured between positive and negative potential scan directions.

Figure S3. LSVs based on mass activities of the Pt(*w*-MeIm), Pt(*w/o*-MeIm), and Pt/C films on GC electrodes.

Figure S4. SEM images of the Pt(*w*-MeIm) film on GC before and after chronopotentiometry for 20 h.

Figure S5. LSVs, Tafel plots, and chronopotentiometry of the Pt(*w*-MeIm) film on GC electrodes in H₂SO₄ (pH 0.5) and KPi (0.1 M, pH = 7.0) solutions.

Table S1. Comparison of the Pt(*w*-MeIm) electrode with the state-of-the-art Pt-based cathodes with the excellent η^{10} values less than 200 mV for HER performance in 1.0 M KOH media (pH 14).

| Catalysts | Current collectors | Γ_{Pt} / mg cm ⁻² | Fabrication methods | η^{10} / mV | Tafel slope / mV dec ⁻¹ | Stability | Ref. |
|---|--------------------|--|------------------------------------|---------------------|------------------------------------|--|------|
| Pt(<i>w</i> -MeIm) | GC | 0.098 | Drop casting/calcination | 60 | 62 | η^{10} increased from 60 to 131 mV after 20 h. | TW |
| Pt | NF | ~1.0 | Electrophoretic | 22 | 31 | At $\eta = 22$ mV, j decreased from 10 to 6 mA cm ⁻² after 48h. | S1 |
| Pt/NiO/Ni | NF | 0.092 | Electrodeposition | 34 | 39 | η^{10} increased from 34 to 55 mV after 24 h. | S2 |
| Pt/Ni | NF | 0.113 | Electrodeposition | 50 | 56 | NA | S2 |
| Pt-Ni ₃ N | Ni mesh | 0.300 | LSV deposition | 50 | 36.5 | At $\eta = 50$ mV, j decreased from 10 to 8 mA cm ⁻² after 24h. | S3 |
| PtO ₂ -Ni(OH) ₂ NS | Ti | 0.0755 | Hydrothermal | 80 70 | 89 | η^{20} remained constant at ~300 mV for 100 h. | S4 |
| PtCo-Co | Ti mesh | 0.0430 | Hydrothermal/calcination | 28 | 35 | j remained constant at 20 mA cm ⁻² for 50 h, but η^{20} was not mentioned. | S5 |
| Pt(111) modified by Ni(OH) ₂ | Pt | NA | Electrodeposition | 138 | 100-130 | At $\eta = 80$ and 110 mV, j remained constant at 3.7 and 7.7 mA cm ⁻² for 2.25 h. | S6 |
| Pt modified by Ni(OH) ₂ | Pt | NA | Chemical deposition | ~45 (η^5) | 75 | NA | S7 |
| Pt _{SA} -Co(OH) ₂ | Ag | 0.059 | Cyclic voltametric deposition | 29 | 35.7 | η^{20} remained constant at 65 mV for 50 h and η^{100} increased from 140 to 150 after 20 h. | S8 |
| Pt ₁₃ Cu ₇₃ Ni ₁₄ /CNF | C felt | 6.653 | Impregnation/galvanic displacement | 67 | 54 | At $\eta = 100$ mV, j decreased by 18% of its initial value after 0.28 h | S9 |
| Pt ₃ Ni ₂ NW-S/C | GC | 0.077 | Drop casting with Nafion | 51 | NA | η^5 increased from 30 to 40 after 5h. | S10 |
| Pt-Ni AS | GC | 0.0170 | Drop casting with Nafion | 27.7 | 27 | NA | S11 |
| Pt ₃ Ni/C nanoframes/Ni(OH) ₂ | GC | 0.0100 | Drop casting with Nafion | 63 (η^5) | NA | NA | S12 |
| Pt NW/SL-Ni(OH) ₂ | GC | 0.0161 | Drop casting with Nafion | 70 ($\eta^{2.5}$) | NA | NA | S13 |

| | | | | | | | |
|--|-------------|---------|--------------------------------|-----------------|-------|---|---------|
| Pt-BP/GR | GC | 0.0143 | Drop casting with Nafion | 21 | 46.9 | NA | S14 |
| Pt _{SA} -NiO/Ni/Ag NW | Flex. cloth | 0.0054 | Hydrothermal/electrodeposition | 26 | 27.1 | η^{20} remained constant at 40 mV for 30 h. | S15 |
| Pt _{SA} -MoSe ₂ | GC | 0.0029 | Drop casting with Nafion | 29 | 41 | NA | S16 |
| Pt _{SA} -N-C | GC | 0.0063 | Drop casting with Nafion | 46 | 36.8 | η^{10} remained constant at 46 mV for 20 h. | S17 |
| Pt _{SA} /AG | GC | 0.0311 | Drop casting with Nafion | 12 | 30.6 | NA | S18 |
| In-Pt _{SA} NW/C | GC | 0.0128 | Drop casting with Nafion | 46 | 32.4 | η^{10} remained constant at 46 mV for 5 h. | S19 |
| Hcp-Pt-Ni/C | GC | 0.0076 | Drop casting with Nafion | 65 | 78 | At $\eta = 65$ mV, j decreased from 10 to 5 mA cm ⁻² after 1h. | S20 |
| PtNi-O/C | GC | 0.0051 | Drop casting with Nafion | 40 | 78.8 | η^{10} increased from 40 to 100 mV after 10 h. | S21 |
| Pt _{3.6} Ni-S NW/C | GC | 0.0153 | Drop casting with Nafion | 20 | 114.8 | η^5 increased from 15 to 33 mV after 5 h. | S22 |
| PtNi NP/Ni NSA | C cloth | 0.0693 | Drop casting with Nafion | 38 | 42 | η^{20} increased from 50 to 90 mV after 90 h. | S23 |
| Pt ₃ Ni ₃ NW/C-air | GC | 0.0153 | Drop casting with Nafion | 40 | NA | η^5 increased from 30 to 40 mV after 3 h. | S24, 25 |
| Pt ₁ Ru _{1.54} NC/BP | GC | 0.0148 | Drop casting with Nafion | 22 | 19 | At $\eta = 22$ mV, j decreased from 10 to 7 mA cm ⁻² after 20 h. | S26 |
| Pt-Co(OH) ₂ | C cloth | 0.3900 | Electrodeposition | 32 | 70 | η^5 increased from 32 to 90 mV after 20 h, | S27 |
| Pt-Ni octahedra/C | GC | 0.0062 | Drop casting with Nafion | 70 | 59 | η^4 increased from 25 to 50 mV after 1 h, | S28 |
| Pt-2D-(NiOH) ₂ /C | GC | 0.00113 | Drop casting with Nafion | 180 | 72 | At $\eta = 100$ mV, j decreased by 49% of its initial value after 5.56 h. | S29 |
| PtNiCo alloy nanohexapod/C | GC | 0.0100 | Drop casting with Nafion | 22 (η^5) | NA | NA | S30 |

GC: Grassy carbon, TW: this work, NA: not available, NS: nanosheet, Pt_{SA}:Pt single atom, CNF: carbon nanofiber, NW: nanowires, AS: anisotropic, SL: single layered, BP: black phosphorous, GR: graphite, N-C: nitrogen doped carbon, AG: aniline-stacked graphene, Hcp: hexagonal close-packed superstructure, NP nanoparticle, NSA: nanosheet array, air: the Pt₃Ni₃ NW/C catalyst is thermally annealed in air, NC: nanocrystals, , 2D: two dimensional.

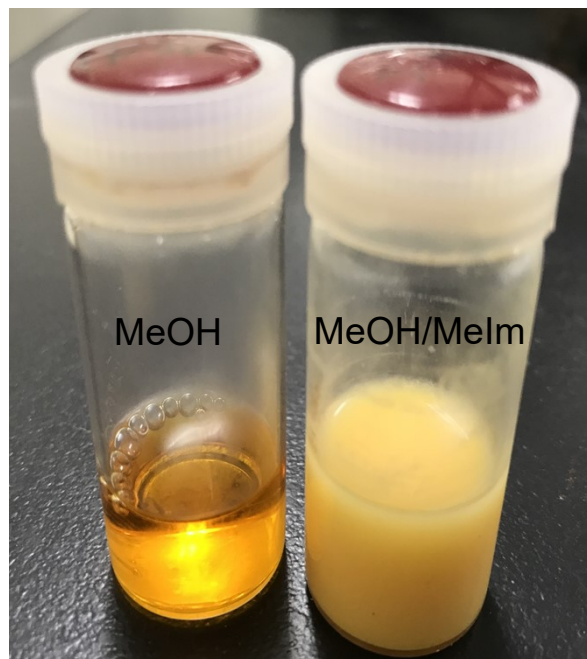


Figure S1. Photos of H_2PtCl_6 (50 mM) precursor solutions in MeOH (left) and MeOH/MeIm (right).

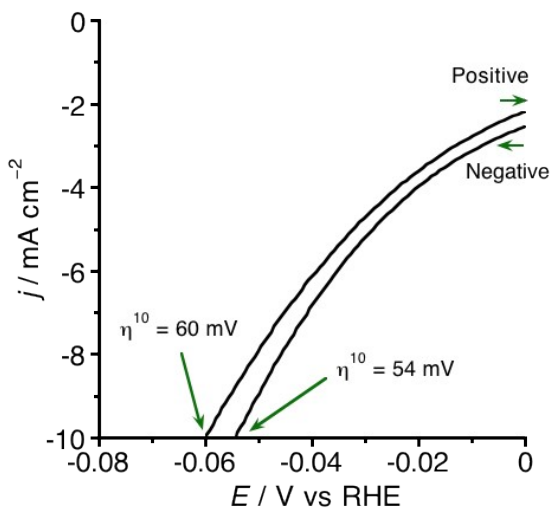


Figure S2. Comparison of LSVs (iR corrected) of the Pt(*w*-MeIm) film on a GC electrode (1.0 cm^2 of geometric area, $\Gamma_{\text{Pt}} = 0.5\text{ }\mu\text{mol (97.5 }\mu\text{g)}\text{ cm}^{-2}$) in 1.0 M KOH solutions (pH 14.0) as measured between positive and negative potential scan directions at a scan rate of 5 mV s^{-1} . The η^{10} value (54 mV) of the Pt(*w*-MeIm) electrode for HER measured in the negative scan direction was lower than (60 mV) in the positive scan direction due to contribution of the current by reduction of the material itself.

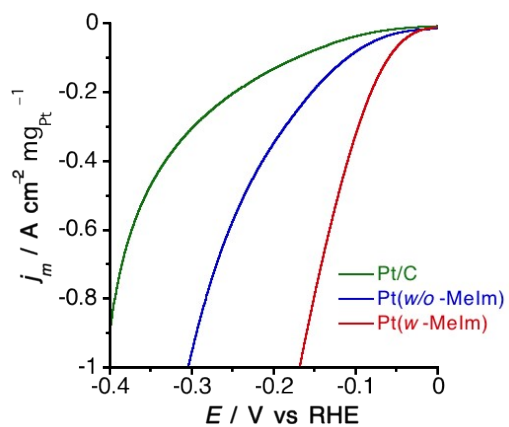


Figure S3. LSVs based on mass activities of the Pt(*w*-MeIm), Pt(*w/o*-MeIm), and Pt/C films on GC electrodes. (1.0 cm^2 of geometric area, $\Gamma_{\text{Pt}} = 0.5 \mu\text{mol cm}^{-2}$) in 1.0 M KOH solutions (pH 14.0) at a scan rate of 5 mV s⁻¹ (The films are shown by different colors in the figure).

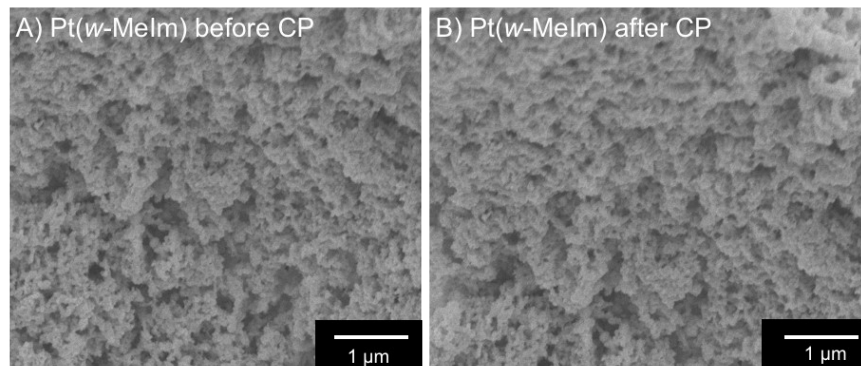


Figure S4. SEM images (top view) of Pt(*w*-MeIm) on GC (A) before and (B) after chronopotentiometry (CP) at 10 mA cm^{-2} for 20 h.

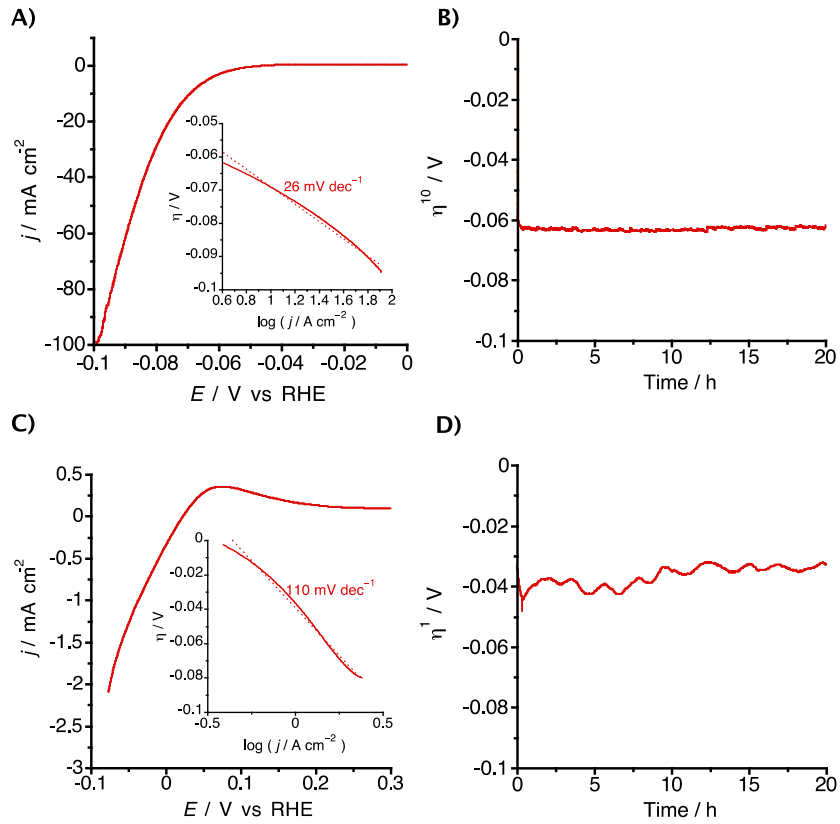


Figure S5. LSVs (iR corrected) of the Pt(*w*-MeIm) film on GC electrodes (1.0 cm^2 of geometric area, $\Gamma_{\text{Pt}} = 0.5 \mu\text{mol}$ ($97.5 \mu\text{g}$) cm^{-2}) in (A) a H_2SO_4 (pH 0.5) and (C) phosphate buffer (0.1 M, pH = 7.0) solutions as measured in the positive potential scan direction at a scan rate of 5 mV s^{-1} . Insets show Tafel plots (solid lines), Tafel slopes (dashed lines), and values based on the LSV data. Chronopotentiograms of η^{10} and η^1 for -10 and -1.0 mA cm^{-2} of current densities for HER in (B) a H_2SO_4 (pH 0.5) and (D) phosphate buffer (0.1 M, pH = 7.0) solutions, respectively.

References:

- S1 C. Panda, P. W. Menezes, S. Yao, J. Schmidt, C. Walter, J. N. Hausmann and M. Driess, *J. Am. Chem. Soc.*, 2019, **141**, 13306–13310.
- S2 Z. J. Chen, G. X. Cao, L. Y. Gan, H. Dai, N. Xu, M. J. Zang, H. Bin Dai, H. Wu and P. Wang, *ACS Catal.*, 2018, **8**, 8866–8872.
- S3 Y. Wang, L. Chen, X. Yu, Y. Wang and G. Zheng, *Adv. Energy Mater.*, 2017, **7**, 1601390.
- S4 L. Xie, X. Ren, Q. Liu, G. Cui, R. Ge, A. M. Asiri, X. Sun, Q. Zhang and L. Chen, *J. Mater. Chem. A*, 2018, **6**, 1967–1970.
- S5 Z. Wang, X. Ren, Y. Luo, L. Wang, G. Cui, F. Xie, H. Wang, Y. Xie and X. Sun, *Nanoscale*, 2018, **10**, 12302–12307.
- S6 R. Subbaraman, D. Tripkovic, D. Strmcnik, K. C. Chang, M. Uchimura, a P. Paulikas, V. Stamenkovic and N. M. Markovic, *Science*, 2011, **334**, 1256–1260.
- S7 N. Danilovic, R. Subbaraman, D. Strmcnik, K. C. Chang, A. P. Paulikas, V. R. Stamenkovic and N. M. Markovic, *Angew. Chemie - Int. Ed.*, 2012, **51**, 12495–12498.
- S8 K. L. Zhou, C. Wang, Z. Wang, C. B. Han, Q. Zhang, X. Ke, J. Liu and H. Wang, *Energy Environ. Sci.*, 2020, **13**, 3082–3092.
- S9 Y. Shen, A. C. Lua, J. Xi and X. Qiu, *ACS Appl. Mater. Interfaces*, 2016, **8**, 3464–3472.
- S10 P. Wang, X. Zhang, J. Zhang, S. Wan, S. Guo, G. Lu, J. Yao and X. Huang, *Nat. Commun.*, 2017, **8**, 14580.
- S11 Z. Zhang, G. Liu, X. Cui, B. Chen, Y. Zhu, Y. Gong, F. Saleem, S. Xi, Y. Du, A. Borgna, Z. Lai, Q. Zhang, B. Li, Y. Zong, Y. Han, L. Gu and H. Zhang, *Adv. Mater.*, 2018, **30**, 1801741.
- S12 C. Chen, Y. Kang, Z. Huo, Z. Zhu, H. W., H. L. Xin, J. D. Snyder, D. Li, J. A. Herron, M. Mavrikakis, M. Chi, K. L. More, Y. Li, N. M. Markovic, G. A. Somojai, P. Yang and V. R. Stamenkovic, *Science (80-.).*, 2014, **343**, 1339–1343.
- S13 H. Yin, S. Zhao, K. Zhao, A. Muqsit, H. Tang, L. Chang, H. Zhao, Y. Gao and Z. Tang, *Nat. Commun.*, 2015, **6**, 6430.
- S14 X. Wang, L. Bai, J. Lu, X. Zhang, D. Liu, H. Yang, J. Wang, P. K. Chu, S. Ramakrishna and X. F. Yu, *Angew. Chemie - Int. Ed.*, 2019, **58**, 19060–19066.
- S15 K. L. Zhou, Z. Wang, C. B. Han, X. Ke, C. Wang, Y. Jin, Q. Zhang, J. Liu, H. Wang and H. Yan, *Nat. Commun.*, 2021, **12**, 3783.
- S16 Y. Shi, Z. R. Ma, Y. Y. Xiao, Y. C. Yin, W. M. Huang, Z. C. Huang, Y. Z. Zheng, F. Y. Mu, R. Huang, G. Y. Shi, Y. Y. Sun, X. H. Xia and W. Chen, *Nat. Commun.*, 2021, **12**, 3021.
- S17 S. Fang, X. Zhu, X. Liu, J. Gu, W. Liu, D. Wang, W. Zhang, Y. Lin, J. Lu, S. Wei, Y. Li and T. Yao, *Nat. Commun.*, 2020, **11**, 1029.
- S18 S. Ye, F. Luo, Q. Zhang, P. Zhang, T. Xu, Q. Wang, D. He, L. Guo, Y. Zhang, C. He, X. Ouyang, M. Gu, J. Liu and X. Sun, *Energy Environ. Sci.*, 2019, **12**, 1000–1007.
- S19 Y. Zhu, X. Zhu, L. Bu, Q. Shao, Y. Li, Z. Hu, C. Te Chen, C. W. Pao, S. Yang and X. Huang, *Adv. Funct. Mater.*, 2020, **30**, 2004310.

- S20 Z. Cao, Q. Chen, J. Zhang, H. Li, Y. Jiang, S. Shen, G. Fu, B. A. Lu, Z. Xie and L. Zheng, *Nat. Commun.*, 2017, **8**, 15131.
- S21 Z. Zhao, H. Liu, W. Gao, W. Xue, Z. Liu, J. Huang, X. Pan and Y. Huang, *J. Am. Chem. Soc.*, 2018, **140**, 9046–9050.
- S22 Z. Liu, J. Qi, M. Liu, S. Zhang, Q. Fan, H. Liu, K. Liu, H. Zheng, Y. Yin and C. Gao, *Angew. Chemie - Int. Ed.*, 2018, **57**, 11678–11682.
- S23 L. Xie, Q. Liu, X. Shi, A. M. Asiri, Y. Luo and X. Sun, *Inorg. Chem. Front.*, 2018, **5**, 1365–1369.
- S24 P. Wang, K. Jiang, G. Wang, J. Yao and X. Huang, *Angew. Chemie*, 2016, **128**, 13051–13055.
- S25 P. Wang, K. Jiang, G. Wang, J. Yao and X. Huang, *Angew. Chemie - Int. Ed.*, 2016, **55**, 12859–12863.
- S26 Y. Li, W. Pei, J. He, K. Liu, W. Qi, X. Gao, S. Zhou, H. Xie, K. Yin, Y. Gao, J. He, J. Zhao, J. Hu, T. S. Chan, Z. Li, G. Zhang and M. Liu, *ACS Catal.*, 2019, 10870–10875.
- S27 Z. Xing, C. Han, D. Wang, Q. Li and X. Yang, *ACS Catal.*, 2017, **7**, 7131–7135.
- S28 R. Kavian, S. Il Choi, J. Park, T. Liu, H. C. Peng, N. Lu, J. Wang, M. J. Kim, Y. Xia and S. W. Lee, *J. Mater. Chem. A*, 2016, **4**, 12392–12397.
- S29 L. Wang, Y. Zhu, Z. Zeng, C. Lin, M. Giroux, L. Jiang, Y. Han, J. Greeley, C. Wang and J. Jin, *Nano Energy*, 2017, **31**, 456–461.
- S30 A. Oh, Y. J. Sa, H. Hwang, H. Baik, J. Kim, B. Kim, S. H. Joo and K. Lee, *Nanoscale*, 2016, **8**, 16379–16386.